

What can be learnt from dielectric relaxation spectroscopy about ion solvation and association?*

Richard Buchner[‡]

*Institute for Physical and Theoretical Chemistry, University of Regensburg,
D-93040 Regensburg, Germany*

Abstract: Ion solvation and ion association are key features of ion–solvent interactions, and their balance largely determines structure, thermodynamics, and dynamics of electrolyte solutions. Despite being studied for many years with various techniques, these effects are still intriguing because too often results obtained with different methods—each having its individual merits and limitations—cannot be connected properly due to lacking information.

In this contribution, we would like to bring dielectric relaxation spectroscopy (DRS) as a further tool for solution studies to the attention of the audience. The principles of DRS and the required instrumentation are briefly introduced. The major focus will be on the kind of results obtained with this technique regarding ion solvation and association and how this information compares with results obtained from other techniques.

Keywords: dielectric relaxation spectroscopy; relaxation time; dipole moment; electrolytes; ion solvation; hydration; ion association; equilibrium constants; speciation.

INTRODUCTION

Ion–ion and ion–solvent interactions have been part of the focus of solution chemistry since its early days. A significant body of information has been accumulated showing the importance of these phenomena in many areas, from geochemistry via biological processes to technical applications [1,2]. Nevertheless, many open questions remain or have actually been put forward by novel molecular-level experiments and computer simulations. One of them is the connection between coordination numbers, as obtained from computer simulations [3] and scattering experiments [4], and effective hydration numbers determined with various methods [5–8]. Regarding ion association, views in the literature range from no ion association at all for most aqueous electrolytes [5], including even for 2:2 electrolytes in water [9], to the claim that even in the case of NaCl(aq) all ions are in the form of hydrated clusters and “these clusters behave as strongly bound units where the cation and anion in each cluster are inseparable” [6]. The consensus seems to be somewhere in between these extremes but the discussion on the merits and shortcomings of the various methods used to study ion association is still open [10,11].

*Paper based on a presentation at the 30th International Conference on Solution Chemistry (ICSC 30), 16–20 July 2007, Perth, Australia. Other presentations are published in this issue, pp. 1195–1347.

[‡]E-mail: Richard.Buchner@chemie.uni-regensburg.de

PRINCIPLES OF DIELECTRIC RELAXATION SPECTROSCOPY

Dielectric relaxation spectroscopy (DRS) probes polarization as the response of the sample to a time-dependent electric field [12,13]. For electrolyte solutions, polarization essentially originates from the orientational fluctuations of permanent dipoles (solvent molecules, ion pairs), from intramolecular polarizability and from ion motion. It can be investigated either in the time domain or as a function of the frequency ν of a harmonic field. In the latter case, the response is conveniently expressed in terms of the complex total (relative) permittivity

$$\hat{\eta}(\nu) = \hat{\epsilon}(\nu) - i\kappa / (2\pi\epsilon_0\nu) = \epsilon'(\nu) - i(\epsilon''(\nu) + \kappa / (2\pi\epsilon_0\nu)) \quad (1)$$

where the complex (relative dielectric) permittivity, $\hat{\epsilon}(\nu) = \epsilon'(\nu) - i\epsilon''(\nu)$, summarizes the effects of dipole fluctuations and intramolecular polarizability, whereas the conductivity, κ , of the sample gives rise to an independent loss contribution; ϵ_0 is the permittivity of vacuum. Typical dielectric spectra are shown in Figs. 1 and 2. The (relative) permittivity $\epsilon'(\nu)$ expresses how far the studied ensemble of dipoles is able to follow the external field at a certain ν . At low frequencies, molecular motions are much faster and the sample is always at equilibrium, thus the static permittivity (dielectric constant) $\epsilon = \lim_{\nu \rightarrow 0} \epsilon'(\nu)$ is obtained. With increasing ν , the dipoles lag more and more behind the changing field, leading to the dispersion of $\epsilon'(\nu)$. Finally, at very high frequencies, only intramolecular polarizability contributes and $\epsilon_\infty = \lim_{\nu \rightarrow \infty} \epsilon'(\nu)$ is reached (Figs. 1a, 2). In the dispersion region of $\epsilon'(\nu)$, energy is dissipated in the sample, giving rise to the dielectric loss $\epsilon''(\nu)$ (Figs. 1b, 2).

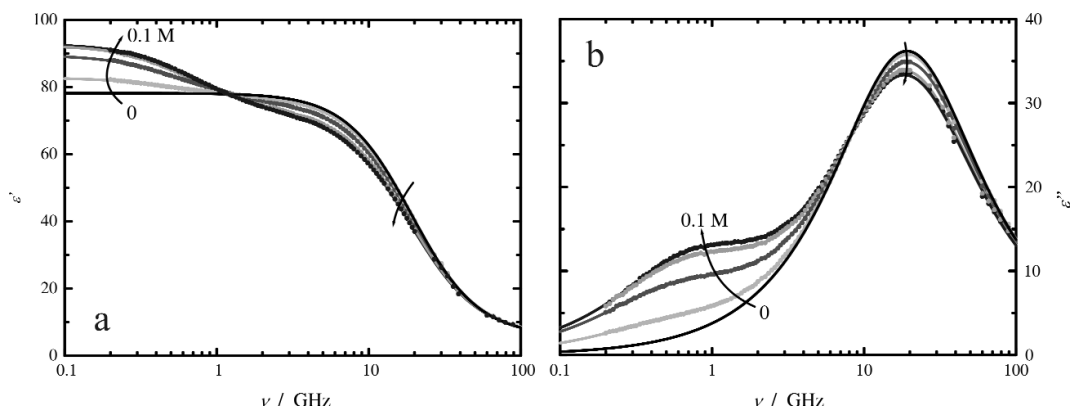


Fig. 1 (a) Dielectric permittivity, $\epsilon'(\nu)$, and (b) loss, $\epsilon''(\nu)$, spectra of aqueous $\text{Al}_2(\text{SO}_4)_3$ solutions at 25 °C and concentrations $c = 0, 0.0115, 0.0425, 0.0855,$ and 0.1054 M [14]. The emergence of a solute relaxation at ~ 0.8 GHz on top of the decreasing solvent process at ~ 18 GHz is clearly seen.

The time scale accessible to dielectric spectroscopy—albeit not with a single instrument—extends from tens of femtoseconds to hours, corresponding to frequencies from the far infrared (THz) region to mHz, which makes DRS probably the technique with the widest dynamic range. Not surprisingly, DRS is applied in many fields of research [12]. For solutions far from glass transition, as discussed in this contribution, the time scale for molecular motions is in the order of tens of femtoseconds to nanoseconds, so that experiments should be conducted at frequencies in the MHz to THz region [13,16]. Despite considerable advances over the last decade, this region is still not easy to access and reasonable-quality instrumentation is commercially available only for $\nu \leq 20$ GHz. Broad-band coaxial equipment can only be used up to ~ 20 GHz with sufficient accuracy. In the THz region beyond ~ 100 GHz, broad-band experiments again become possible, now using free-space wave propagation as in conventional infrared spectroscopy. But the THz range is just now becoming

reasonably easily accessible, and electrolyte studies are still scarce. Between ~20 and ~100 GHz, waveguide instruments with limited bandwidth have to be used, which make measurements cumbersome and time-consuming. This explains why only few laboratories use DRS in solution studies so far. The spectrum of Fig. 2 exemplifies this problem. Here, the data for $\nu \leq 7$ GHz were obtained with a coaxial-line time-domain reflectometer (TDR), whereas four waveguide interferometers (IFMs) cover the region between 8.5 and 89 GHz [15]. Readers interested in measurement techniques are referred to recent reviews [17,18].

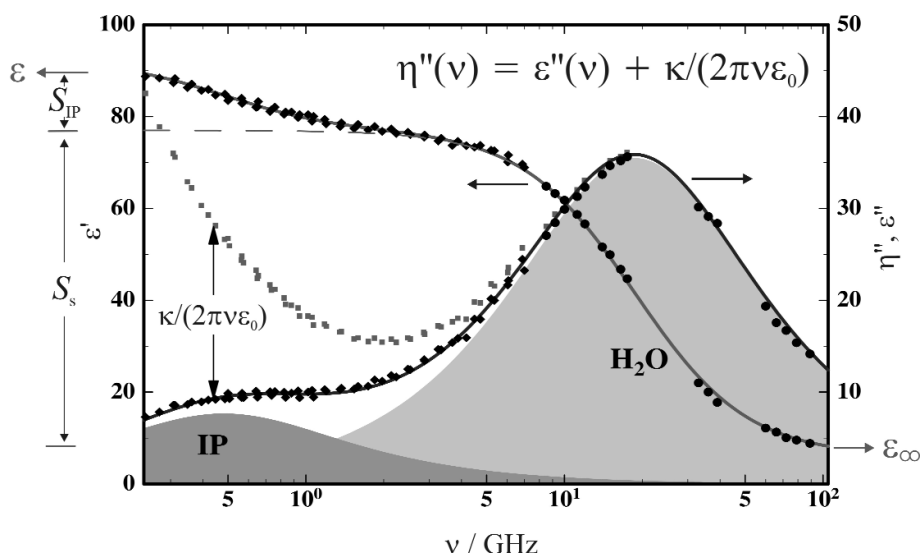


Fig. 2 Dielectric permittivity, $\epsilon'(\nu)$, and loss, $\epsilon''(\nu)$, spectrum of 0.0345 M $\text{La}[\text{Fe}(\text{CN})_6]_3(\text{aq})$ at 25 °C obtained with TDR (diamonds) and IFM (circles). Squares indicate the conductivity contribution to the total loss, $\eta''(\nu)$ [15].

In order to extract quantitative information from the dielectric spectra, an appropriate (formal) mathematical description has to be found and then scrutinized for its physical relevance. Generally, it is possible to decompose $\hat{\epsilon}(\nu)$ into a sum of n individual relaxations $i = 1 \dots n$ according to eq. 2, see Fig. 2 [19].

$$\hat{\epsilon}(\nu) = \sum_{i=1}^n \frac{S_i}{1 - (i2\pi\nu\tau_i)^{1-\alpha_i} \beta_i} + \epsilon_\infty; \quad (i^2 = -1) \quad (2)$$

Each process is characterized by its amplitude (relaxation strength) S_i , its relaxation time τ_i ($= 1/2\pi\nu_i^{\text{peak}}$ for $\beta_i = 1$, ν_i^{peak} being the peak frequency of the corresponding loss contribution), and eventual band-shape parameters $0 \leq \alpha_i < 1$ and $0 < \beta_i \leq 1$. The limiting case $\alpha_i = 0$ and $\beta_i = 1$ is the Debye relaxation which corresponds to an exponential polarization decay and has the smallest bandwidth possible for an individual relaxation process [12]. Due to overlapping contributions within the limited frequency range covered by experiment, the fitting of solution spectra is usually not trivial. Therefore, in addition to numerical arguments based on the quality of the fit and the number of adjustable parameters, physical criteria based on information from other techniques should be included in the selection of the fitting model [19].

For electrolyte solutions in molecular solvents, the amplitude S_i of relaxation i is directly connected to the concentration, c_i , of the reorienting dipole

$$S_i = \frac{\varepsilon}{3[\varepsilon + (1 - \varepsilon)A_i]} \times \frac{N_A}{k_B T \varepsilon_0} \times \frac{g_i \mu_i^2}{(1 - \alpha_i f_i)^2} \times c_i \quad (3)$$

In eq. 3, μ_i is the dipole moment and α_i the polarizability of the dipole [20]. N_A , k_B , and T have their usual meaning; expressions for the factors of the cavity field, A_i , and the reaction field, f_i , are given in the paper of Barthel et al. [20]. The empirical factor g_i can be considered as a generalized Kirkwood factor for dipole mixtures as it takes possible orientational correlations among the dipoles of species i into account. For dipolar solute species like ion pairs, $g_i = 1$ can be reasonably assumed, so that the concentration c_i of the relaxing species is immediately accessible provided reasonable information on its dipole moment and geometry is available. For the solvent, the situation is usually not so straightforward as generally $g_i \neq 1$. Here, it is convenient to normalize $S_i(c)$ to the amplitude of the pure solvent, $S_i(0)$, so that the effective concentration $c_i^{\text{eff}}(c) = c_i(c) \times g_i(c)/g_i(0)$ is deduced from the solvent amplitudes [21].

Discussion of relaxation times is more subtle as *a priori* DRS probes cooperative dynamics and not the motion of individual dipoles. This is clearly seen in the dependence of the relaxation time of H-bonding solvents on electrolyte concentration, which indicates that here the rearrangement of the H-bond system is probed (Fig. 3 and the discussion given below). However, for dipolar aprotic solvents, such as acetonitrile or *N,N*-dimethylformamide (DMF, Fig. 3c), as well as for ion pairs, dielectric relaxation is dominated by rotational diffusion of the individual dipoles. In this case,

$$\tau_i^{\text{or}} = \tau_i \times (2\varepsilon + \varepsilon_\infty) / 3\varepsilon g_i = 3V_m f_\perp C \eta / k_B T \quad (4)$$

where τ_i^{or} is the rotational correlation time of the dipole, assumed to be an ellipsoid rotating in a medium of viscosity η [13]. V_m is the volume of the dipole, and f_\perp accounts for its deviation from a sphere. The parameter C reflects the hydrodynamic coupling between the reorienting molecule and its environment, with $C = 1$ for *stick* and $C = 1 - f_\perp^{-2/3}$ for *slip* boundary conditions.

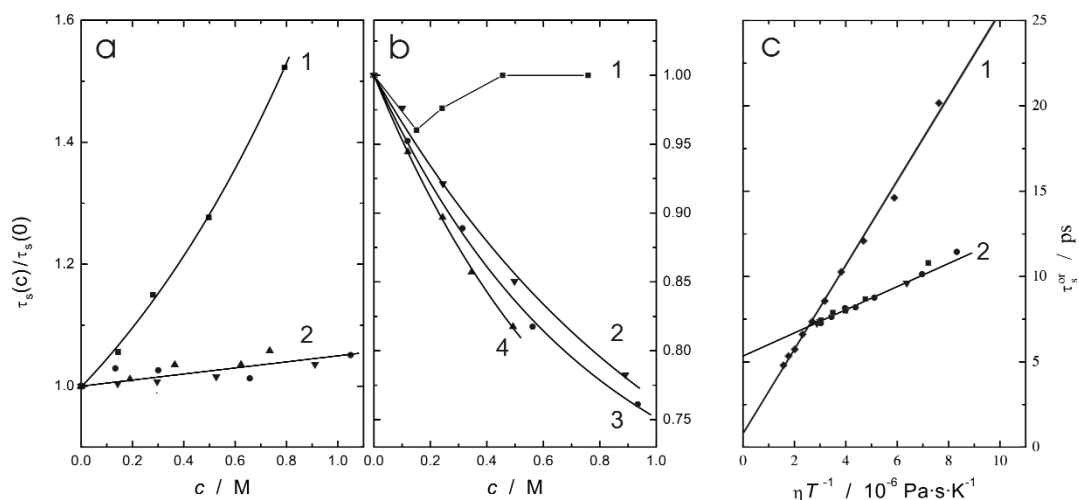


Fig. 3 (a) and (b) Relative bulk-solvent relaxation times, $\tau_s(c)/\tau_s(0)$, of formamide (a) and NMF (b) as a function of electrolyte concentration, c , in solutions of Bu_4NClO_4 (■), LiClO_4 (●), NaClO_4 (▼) and NaCl (▲) at 25 °C. (c) Rotational correlation time, τ_s^{or} , of DMF as a function of η/T for these electrolytes (curve 2) and for pure DMF (curve 1) [22,23].

ION SOLVATION

Possible effects of dissolved ions on the solvent spectrum are (i) a shift of solvent relaxation time (Fig. 3), monitoring the influence of the ions on structure and dynamics of the bulk solvent; (ii) a reduction of its dispersion amplitude, S_s (Figs. 1, 2); and (iii) the emergence of a new solvent relaxation. The last two effects essentially reflect solvation, i.e., direct ion–solvent interactions. Whereas (i) and (ii) are always observed, albeit with considerably differing magnitude depending on the solvent and the electrolyte [13,16], up to now new solvent relaxations have only been observed for solutions of large hydrophobic ions in water [21,24,25].

Figure 3 shows the influence of 1:1 electrolytes on the solvent relaxation times, τ_s , of (a) formamide, (b) *N*-methylformamide (NMF), and (c) DMF; here, the rotational correlation time τ_s^{or} is shown. In all cases, the viscosity of the solutions increases with electrolyte concentration, but only for DMF the rotational correlation time calculated from τ_s is proportional to η as expected from eq. 4 (Fig. 3c). Such behavior is typical for dipolar aprotic solvents where solvent relaxation is dominated by the rotational diffusion of molecular dipoles [16,22]. Since τ_s^{or} only depends on solution viscosity but not on the specific electrolyte, it can be inferred that the impact of the solvated ions on the structure of the bulk solvent is negligible.

In the case of H-bonding solvents, DRS essentially probes the cooperative rearrangement of the H-bond system and relaxation is dominated by the “wait-and-switch” mechanism [26–28]. For these liquids, the relaxation time is governed by the period for which a given ensemble of H-bond partners has to wait until favorable conditions for the reorientation of a molecular dipole exist. This situation is created by an approaching “defect” in the H-bond system, generally an additional solvent or solute particle, which modifies the potential energy surface through its interactions with the ensemble and simultaneously offers a site for the formation of a new H bond [26].

Depending on the relative strength of ion–solvent versus solvent–solvent interactions and on the structure of the H-bond system, dissolved ions may either be “neutral” toward the dynamics of the bulk solvent (Fig. 3a, curve 2), act as “defects” catalyzing dipole reorientation (Fig. 3b, curves 2–4) or even act as shields against the attack of “defects” for the solvent molecules in their primary solvation shell (Fig. 3a, curve 1) [22,23,29]. For sufficiently large hydrophobic solutes in water, the shielding effect is so pronounced that the H_2O molecules in the primary hydration sphere are detectable as a separate relaxation process with $\tau_s^{\text{slow}} \approx 3\tau_s^{\text{bulk}}$ [21,24,25].

In contrast to the moderate shielding effect exerted by large, weakly interacting ions in H-bond solvents, strong ion-dipole forces created by an ion with high surface-charge density reduce the dynamics of surrounding solvent molecules for all solvent classes. In this case, the slowing down may be so strong that the affected solvent molecules are effectively “frozen” (irrotationally bound) on the DRS time scale and cannot be detected anymore. In addition to the trivial dilution of the solvent dipole density by the added electrolyte, this phenomenon is usually the major reason for the decrease of the solvent dispersion amplitude, S_s , with increasing c (Figs. 1, 2).

From $S_s(c)$, after correction for kinetic depolarization [19], the effective solvent concentration, $c_s^{\text{eff}}(c)$, can be calculated with eq. 3. Comparison of $c_s^{\text{eff}}(c)$ with the analytical solvent concentration, $c_s^{\circ}(c)$, yields the number Z_{ib} of irrotationally bound (frozen) solvent molecules

$$Z_{\text{ib}} = \left(c_s^{\circ} - c_s^{\text{eff}} - c_s^{\text{slow}} \right) / c \quad (5)$$

as an effective solvation number of the electrolyte. In eq. 5, $c_s^{\text{slow}}(c)$ is the amount of solvent eventually detected as a separate solute-induced relaxation—so far only observed for hydrophobic solutes in water [21,24,25]. $c_s^{\text{slow}}(c)$ is directly accessible from the corresponding dispersion amplitude with the help of eq. 3 and allows the definition of an analogous hydrophobic hydration number, $Z_{\text{slow}} = c_s^{\text{slow}}/c$ [21].

Based on the observation that Cl^- and Br^- do not “freeze” the H_2O molecules in their primary hydration shell [21], splitting of Z_{ib} into ionic contributions was possible for a series of aqueous electrolytes. Typical results are shown in Fig. 4, and infinite dilution values, $Z_{\text{ib}}(0)$, are summarized in Table 1, together with first-shell coordination numbers, CN . Depending on the ion, $Z_{\text{ib}}(0)$ may be smaller than CN or significantly larger. For the large cations K^+ and Cs^+ , as well as for most univalent anions, even $Z_{\text{ib}}(0) = 0$ is observed. On the other hand, $Z_{\text{ib}}(c) \gg CN$ for di- and trivalent cations. This clearly indicates that for $Z_{\text{ib}}(c)$, the strength of ion–solvent interactions is decisive and not the packing effects that dominate CN .

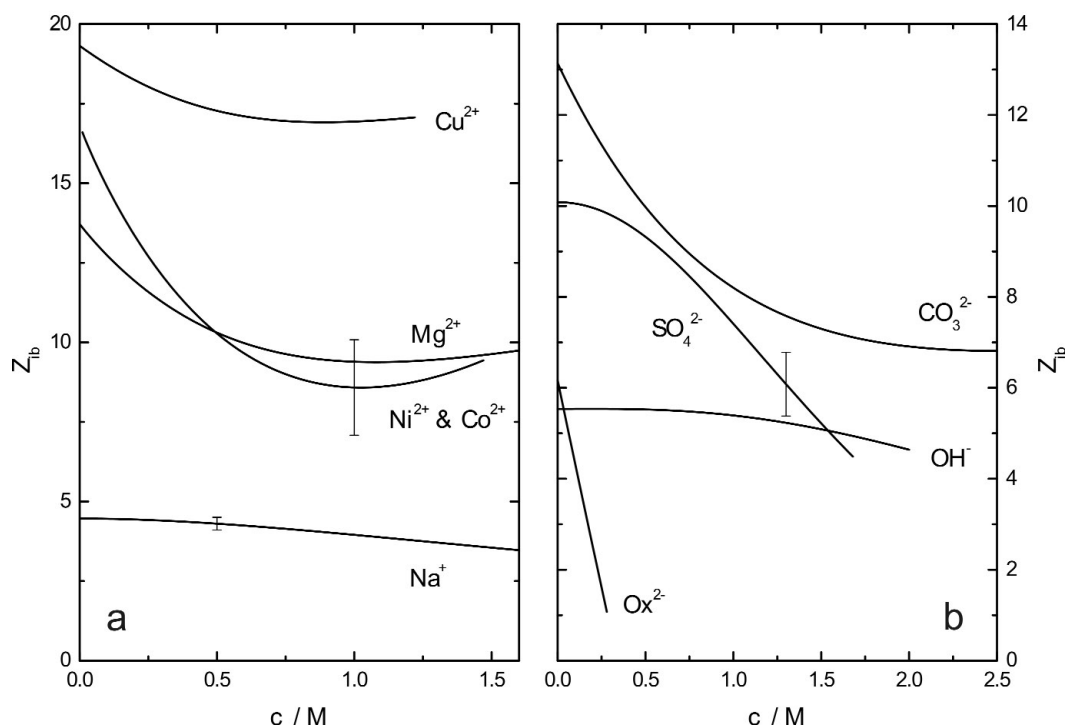


Fig. 4 Concentration dependence of the effective hydration number, Z_{ib} , of (a) cations and (b) anions in aqueous electrolytes at 25 °C.

Table 1 Effective hydration numbers, $Z_{\text{ib}}(0)$, and coordination numbers, CN , of inorganic ions at infinite dilution and 25 °C.

Cation	$Z_{\text{ib}}(0)$	CN	Ref.	Anion	$Z_{\text{ib}}(0)$	CN	Ref.
Li^+	8–12	4	[31]	Cl^-	0	6	[13]
Na^+	4.5	6	[13]	Br^-	0	6–8	[29]
K^+	0	8	[32]	I^-	0	8–9	[29]
Cs^+	0	8	[32]	ClO_4^-	0	6–7	[29]
Mg^{2+}	14	6	[19]	NO_3^-	0	6–9	[29]
Co^{2+}	17	6	[33]	SCN^-	0		[29]
Ni^{2+}	17	6	[33]	OH^-	5.5	6–8	[13]
Cu^{2+}	19	6	[34]	SO_4^{2-}	10	7–12	[13]
Al^{3+}	30	6	[14]	CO_3^{2-}	13		[13]

The attractive interactions between cations and water are dominated by electrostatic forces. Due to their high surface-charge density, small and/or highly charged cations will align the molecules S of their primary solvation layer almost perfectly (Fig. 5a). As a result, their dipole moments cancel in the more or less centro-symmetric complex $[MS_{CN}]^{n+}$. With increasing distance from the ion, the strength of its electric field decreases and thermal motions and H_2O-H_2O H bonds become competitive. Thus, the degree of solvent alignment and dipole–dipole compensation decreases. Nevertheless, for the divalent cations of Table 1 the second hydration shell is clearly affected and for Al^{3+} even the third [14]. The marked decrease of $Z_{ib}(c)$ observed for these ions with increasing electrolyte concentration (Fig. 4a) is readily explained by the decreasing average distance of the ions. This leads to an increasing overlap of their electric fields, which compensate each other so that the outer hydration shells “melt”. For Na^+ with its intermediate charge density, the six H_2O molecules in the first hydration layer may wag and rotate around the radial field lines (Fig. 5b) so that on average their dipole moments do not cancel completely, yielding $Z_{ib}(0) = 4.5$. For large cations, such as K^+ , Cs^+ , or Me_4N^+ , the surface-charge density is too weak to align the surrounding solvent dipoles against thermal motions. As a result, solvent exchange is fast in the first hydration shell and $Z_{ib}(0) = 0$.

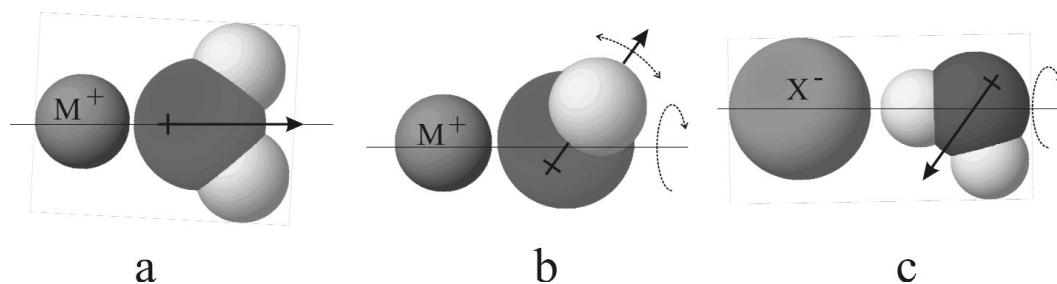


Fig. 5 Preferred orientation of water molecules in the primary hydration shell of (a) cations with high surface-charge density, (b) cations with low surface-charge density, and (c) anions. The arrow indicates the direction of the water dipole moment. For explanations, see the text.

In aqueous solutions, anion–water H bonds are generally comparable in strength to water–water H bonds and electrostatic anion–dipole interactions, leading to a preferred coordination of hydration water via one of the H atoms (Fig. 5c) [4]. Due to the possible rotation of the H_2O molecule around this H bond at best—in the case of strong X^-H_2O bonds—partial compensation of the dipole moments in the complex $[XS_{CN}]^{n-}$ is possible. For most univalent anions, apparently the water–water H bonds dominate, yielding a rapid exchange of H_2O molecules between hydration shell and bulk and thus $Z_{ib}(0) = 0$. Divalent anions show fairly large $Z_{ib}(0)$, but their hydration shells seem to be very sensitive to ion–ion interactions, with that of oxalate, Ox^{2-} , being particularly fragile (Fig. 4b) [35].

For electrolytes in nonaqueous solvents, only a limited number of Z_{ib} values have been reported [16,22,23,30,36]. In line with information from other methods [2], data suggest that anions interact only weakly ($Z_{ib} \approx 0$) with dipolar aprotic solvents, whereas for cations Z_{ib} is correlated with surface-charge density as for water [16,22,36]. The small effective solvation numbers obtained for the four salts (Bu_4NClO_4 , $LiClO_4$, $NaClO_4$, $NaCl$) studied in formamide [23] suggest—in line with τ_s (Fig. 3a)—that the influence of the ions on the H-bond network of this solvent is restricted to the first solvation shell. On the other hand—again in line with τ_s (Fig. 3b)—large infinite-dilution values and a strong concentration dependence of $Z_{ib}(c)$ was observed for electrolyte solutions of the H-bond chain formers NMF [23] and methanol [30]. These effects can be only partly attributed to irrotational bonding and are interpreted as an ion-induced reduction of the average length of the H-bond chains, i.e., as a breakdown of the bulk solvent structure.

ION ASSOCIATION

Despite occasionally raised doubts [5,9], ion association to pairs and eventually larger aggregates seems to be a universal feature of electrolyte systems where attractive ion–ion interactions exceed thermal motion and ion–solvent interactions [2,10,11]. The attraction of oppositely charged ions is dominated by Coulomb forces, so naturally ion association is more pronounced in low-permittivity solvents and between highly charged ions [2], but small yet not negligible amounts of ion pairs have even been detected for various 1:1 and 2:1 electrolytes in water around room temperature [13,31,37,38].

It is commonly thought that ion association is a stepwise process (Fig. 6) following the mechanism suggested by Eigen and Tamm on the basis of ultrasonic relaxation experiments [39]. According to this scheme, the free solvated ions first form in an essentially diffusion-controlled reaction an outer-outer-sphere complex (double-solvent-separated ion pair, 2SIP) where both ions keep their primary solvation shell. In the subsequent—considerably slower—steps, solvent molecules are ejected to form successively an outer-sphere (solvent-shared ion pair, SIP) and then finally an inner-sphere complex (contact ion pair, CIP) in which the anion and cation are in direct contact. Each of these three steps is characterized by its equilibrium constant, K_i , $i = 1, 2, 3$, and the overall equilibrium by the association constant $K_A = K_1 + K_1K_2 + K_1K_2K_3$. Obviously, not all steps of the Eigen mechanism (Fig. 6) are necessarily relevant. Depending on the salt concentration and the balance of ion–ion, ion–solvent, and solvent–solvent interactions the sequence may stop after the first or second step ($\text{Li}_2\text{SO}_4(\text{aq})$ and similar electrolytes [31]), or immediately yield SIP (alkali and alkaline earth perchlorates in acetonitrile [36]) and even CIP (aqueous tetraalkylammonium salts [21]). On the other hand, at least at high salt concentrations, larger aggregates, such as ion triples, may be formed [2,11].

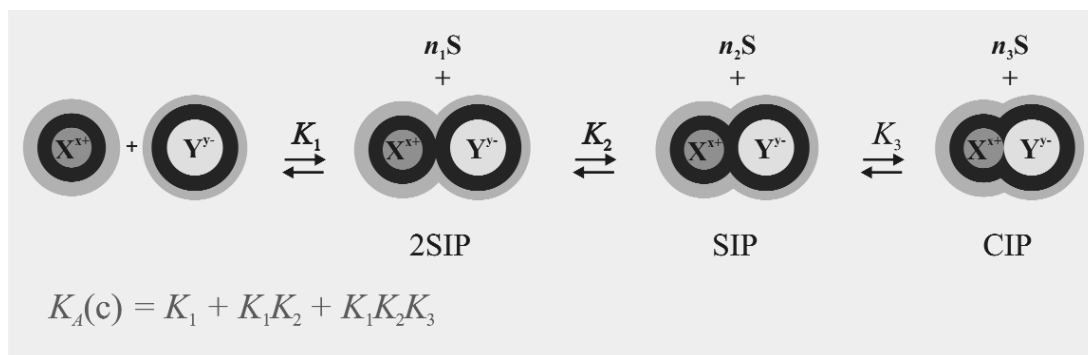


Fig. 6 Scheme of stepwise ion association according to Eigen [39].

The implications of stepwise ion association for the interpretation of experimental data have been discussed in detail in the reviews of Marcus and Hefter [11] and especially Hefter [10]. Here, it may suffice to say that thermodynamic methods and conductivity studies yield the overall association constant K_A , whereas most spectroscopic techniques determine the concentration of CIPs only. Ultrasonic relaxation yields the number of individual relaxation steps/equilibria in the sequence—with the formation of 2SIP from free ions often being too fast to be resolved—but no information on the species formed so that assumptions are necessary to calculate the K_i .

The mayor contribution of DRS to ion-association studies is its ability to detect—at least in principle—all species with dipole moment $\mu_i > 0$, provided their lifetime is at least comparable to their rotational correlation time, τ_i^{or} . Since τ_i^{or} mainly depends on the effective volume of rotation, $V_{\text{m}}f_{\perp}$ (eq. 4), the contributions of 2SIP, SIP, and CIP peak at different frequencies in the dielectric spectrum and the corresponding dispersion amplitudes $S_{2\text{SIP}}$, S_{SIP} , and S_{CIP} immediately yield the corresponding concentrations $c_{2\text{SIP}}$, c_{SIP} , and c_{CIP} with eq. 3. Since the dipole moment of an ion pair essentially de-

depends on the separation of the charges [20], DRS possesses the unique order of $2SIP > SIP > CIP$ in its sensitivity toward ion pairs. However, before these advantages can be used, two independent problems have to be tackled.

The first challenge is finding the proper number of solute relaxations/ion-pair species and the subsequent separation of the individual contributions as bands in dielectric spectra are broad. Generally, the different solute relaxations overlap strongly with each other and with the dominating solvent relaxation(s) (Figs. 1, 2) so that a good-quality formal fit of a certain relaxation model, eq. 2, to a given spectrum may be misleading. This problem is tackled as in all spectroscopic studies of solutions: by scrutinizing a sufficiently large set of spectra for systematic changes with changing concentration or temperature. In the case of $MgSO_4(aq)$ (Fig. 7), the variation of the spectra suggests the presence of three distinguishable solute relaxations (in addition to the two well-known water modes [40]), which was confirmed by the subsequent analysis of the derived amplitudes S_i and relaxation times τ_i [41]. This empirical approach for finding the most probable number n of relaxation processes for the fit (eq. 2) of the spectra will certainly be replaced by the methods of factor analysis in the near future.

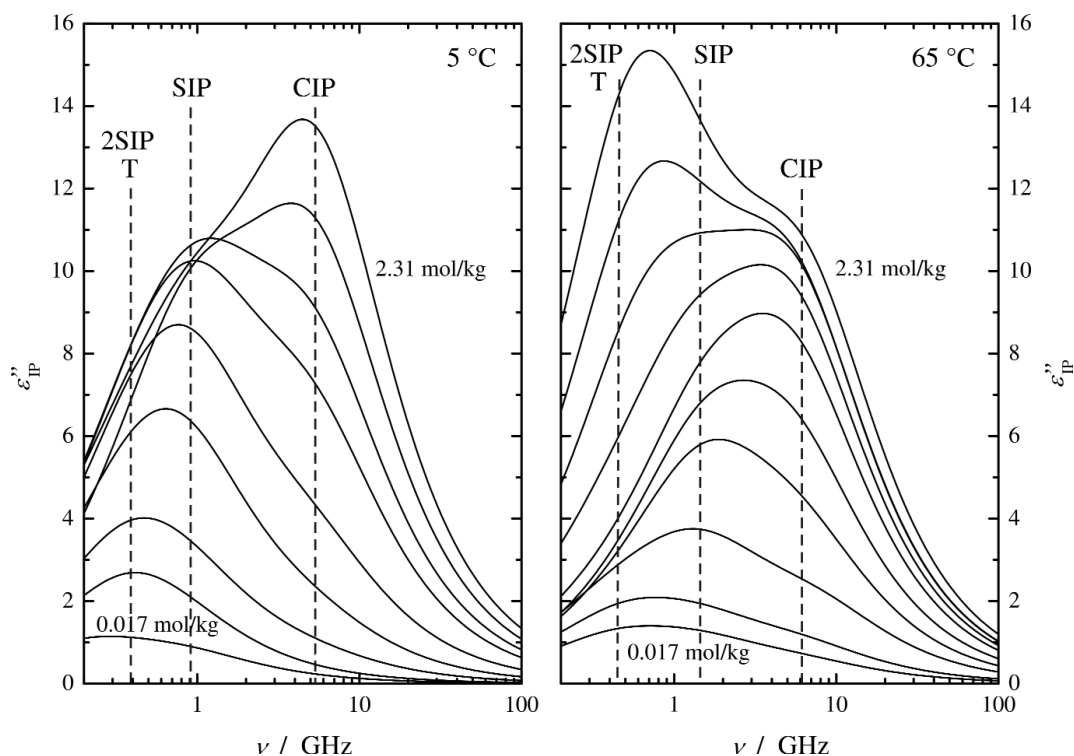


Fig. 7 Solute contribution to the dielectric loss spectra, $\epsilon''_{IP}(\nu)$, of $MgSO_4(aq)$ at (left) 5 and (right) 65 °C. Salt concentrations increase from 0.017 to 2.31 mol/kg [41]. The locations of the loss peaks for the ion-pair types 2SIP, SIP, and CIP are indicated. Accidentally, the peak positions for 2SIP and the polar triple ion $[Mg_2SO_4]^{2+}$ (T) formed at high salt concentrations coincide.

The second problem, the assignment of the resolved relaxations to certain species, is less straightforward. Relaxation times usually provide a first hint, but the quantitative analysis of the solute dispersion amplitudes (Fig. 8a) and subsequent comparison of the results (Figs. 8b, 9) obtained for the possible assignment options with information from other techniques is decisive. The relaxation strengths S_i , $i = 1 \dots 3$, displayed in Fig. 8a are typical for the ion-pair amplitudes extracted from fitting the dielec-

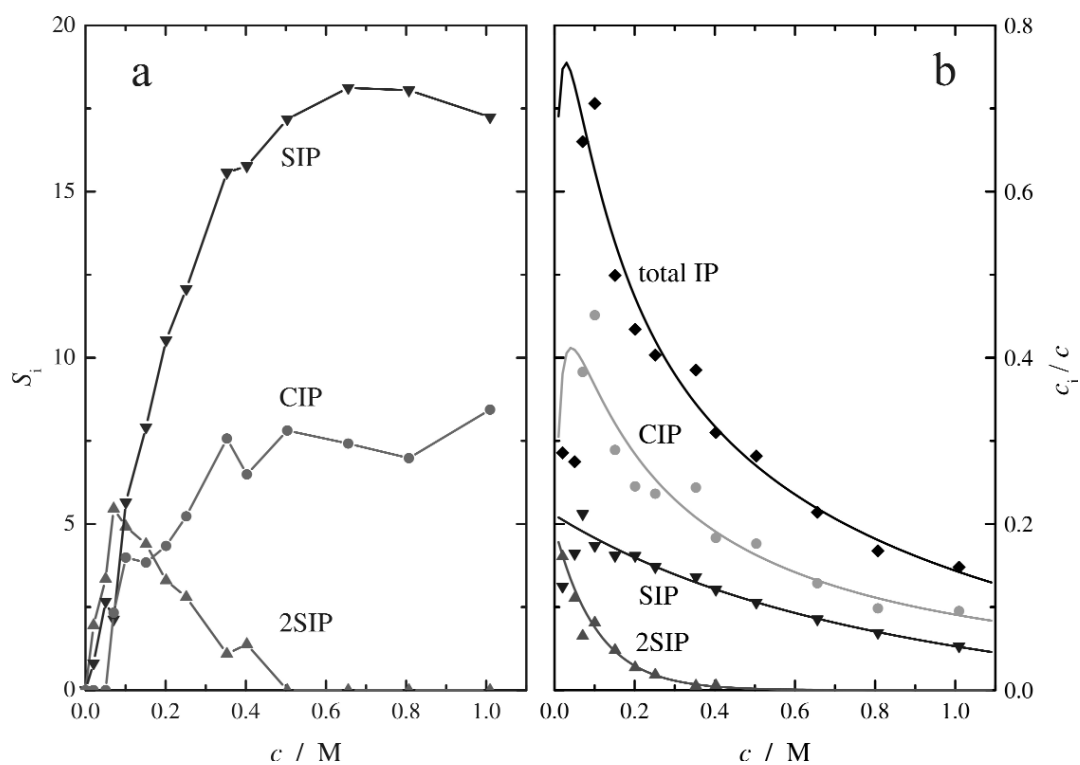


Fig. 8 (a) Detected dispersion amplitudes, $S_i(c)$, of the ion-pair species 2SIP (▲), SIP (▼), and CIP (●) present in $\text{CuSO}_4(\text{aq})$ at 5 °C. (b) Corresponding fractions c_i/c , calculated with eq. 3. The overall degree of association $(c_{2\text{SIP}} + c_{\text{SIP}} + c_{\text{CIP}})/c$ (◆), is also indicated. For the latter, the line was calculated from the fit of eq. 6 to K_A (see Fig. 9a); lines for 2SIP, SIP, and CIP were calculated from appropriately smoothed S_i [34].

tric spectra with eq. 2. In the example $[\text{CuSO}_4(\text{aq})]$ at 5 °C, the slowest relaxation, $i = 1$, *a posteriori* assigned to 2SIP, could not be detected at $c > 0.4$ M. Similarly, the fastest solute relaxation, $i = 3$ and due to CIP, could not be resolved below ~ 0.07 M. The shifted pattern of rise and fall for S_1 , S_2 , and S_3 (Fig. 8a) is already indicative for a three-step equilibrium according to the Eigen mechanism (Fig. 6) so that one tested (and subsequently confirmed) option was the assignment of relaxation 1 to 2SIP, 2 to SIP, and 3 to CIP (since only the procedure should be sketched, we abstain from discussing other tested assignments here).

With the help of the ion-pair dipole moments $\mu_{2\text{SIP}}$, μ_{SIP} , and μ_{CIP} calculated from appropriate models [20,19], the corresponding species concentrations $c_{2\text{SIP}}$, c_{SIP} , and c_{CIP} are then immediately obtained with eq. 3 (Fig. 8b). Since c_{CIP} is—at least in principle—also accessible with NMR, infrared, and Raman spectroscopy, a first cross-check of the assignment is possible at that stage. In the case of $\text{MgSO}_4(\text{aq})$ [42] and $\text{Al}_2(\text{SO}_4)_3(\text{aq})$ [14], good quantitative agreement was found for the contact ion-pair concentrations from DRS, Raman, and NMR. Eberspächer et al. [36] combined infrared spectroscopy and DRS to determine the concentrations of SIP, CIP, and triple ions in solutions of alkaline and alkaline-earth perchlorates in acetonitrile. Unfortunately, good-quality c_{CIP} from spectroscopic studies are rare. This is regrettable as such data would allow calibrating the methods used to calculate the ion-pair dipole moment.

From the electrolyte concentration, c , the derived overall ion-pair concentration, c_{IP} (in the present example: $c_{\text{IP}} = c_{2\text{SIP}} + c_{\text{SIP}} + c_{\text{CIP}}$), and appropriate mass balance equations the concentrations of free cations, c_+ , and anions, c_- , and thus the overall association constant

$$K_A = c_{IP}/c_+c_- \quad (6)$$

are readily accessible as a function of c or corresponding ionic strength, I (Fig. 9a). Extrapolation of $K_A(I)$ to vanishing ionic strength with the help of the Guggenheim-type equation [43]

$$\log K_A = \log K_A^0 - \frac{2A_{DH}|z_+z_-|\sqrt{I}}{1 + A_K\sqrt{I}} + B_K I + C_K I^{3/2} \quad (7)$$

then yields the standard state (infinite dilution) association constant K_A^0 as the final result of the quantitative analysis of ion-pair amplitudes. In eq. 7, A_{DH} is the Debye–Hückel constant for activity coefficients, Y_K ($Y = A, B, \text{ or } C$) are adjustable parameters.

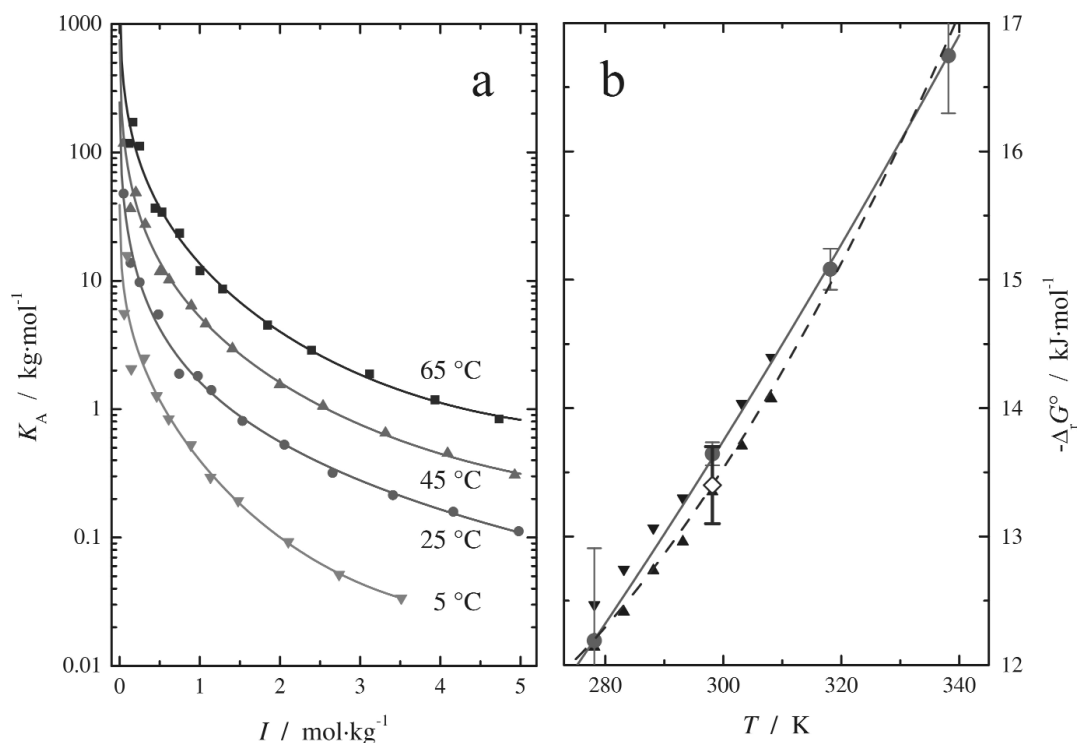


Fig. 9 (a) Molal association constants, K_A (eq. 6), for $\text{CuSO}_4(\text{aq})$ as a function of ionic strength, I , and temperature (symbols) and their fits with eq. 7 (lines) [34]. (b) Corresponding Gibbs energies of ion association, $\Delta_r G^\circ$, from DRS (\bullet , solid line), from recent conductivity measurements (\blacktriangle , \blacktriangledown) [44] and data recommended by IUPAC (\diamond , broken line) [45]. Except for 25 °C, data are shifted in (a) for representational clarity.

K_A^0 or the corresponding standard Gibbs energy of association, $\Delta_r G^\circ = -RT \ln K_A^0$, as well as the eventually derived standard enthalpy, $\Delta_r H^\circ$, entropy, $\Delta_r S^\circ$, and heat capacity, $\Delta_r C_p^\circ$, of ion association can be directly compared with literature data (Fig. 9b) [13,19,34,41]. This comparison provides a stringent test for the chosen assignment of relaxation processes to ion-pair species as usually the K_A^0 values calculated for the different options differ considerably among each other, with only one of them being compatible with data obtained from the generally more accurate thermodynamic measurements and conductivity studies. A typical example is $\text{LiCl}(\text{aq})$ [31]. Here, two solute relaxations were found, so possible combinations of ion-pair species were 2SIP/SIP, 2SIP/CIP, and SIP/CIP, yielding K_A^0 val-

ues of 1.5, ~500, and 35, respectively. Only the result for 2SIP/CIP is compatible with the available literature data (0.81, 2.75, 2.45) [31].

DRS is certainly not the most accurate method to determine the standard-state (infinite dilution) association constant K_A^0 as usually a long extrapolation to infinite dilution is required. Also, as in the above example for LiCl(aq), often several options for assigning relaxations to ion-pair species exist, although not all of them are usually equally plausible. Thus, reference data for K_A^0 are often required for the proper interpretation of DRS spectra. On the other hand, if a proper assignment of solute relaxations to ion-pair species can be made, then DRS provides the most straightforward access to K_A values as a function of electrolyte concentration and/or ionic strength (Figs. 9a, 10). DRS also yields standard-state association constants of good quality even for $K_A^0 < 10$, where thermodynamic methods and conductivity measurements are increasingly unreliable [13,22,24,31].

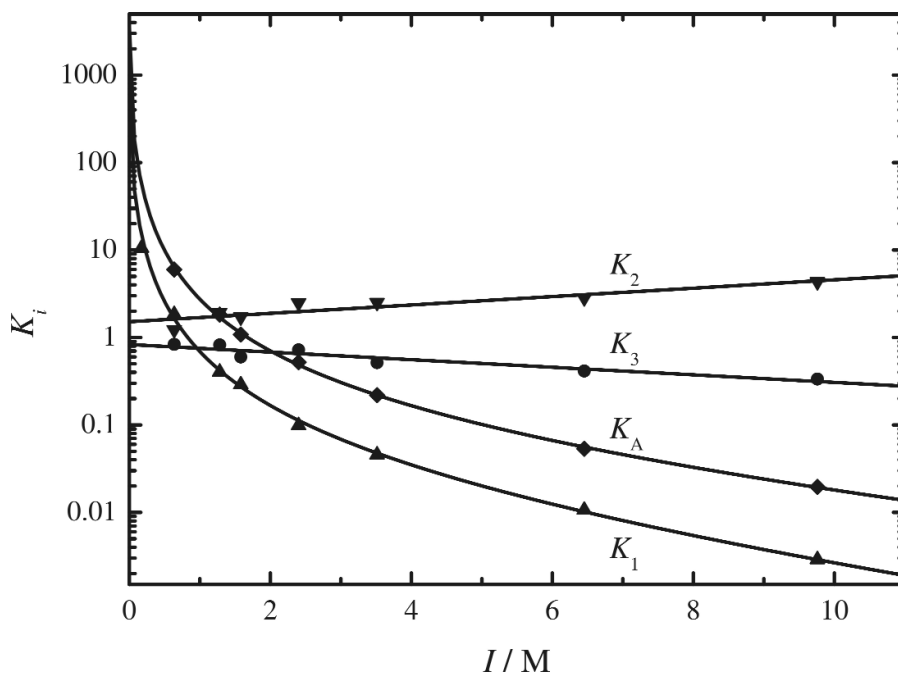


Fig. 10 Molar overall association constants, $K_A = K_1 + K_1K_2 + K_1K_2K_3$, for $\text{Al}_2(\text{SO}_4)_3(\text{aq})$ as a function of ionic strength, I , at 25 °C together with the constituting equilibrium constants for the equilibria between free ions and 2SIP, K_1 , between 2SIP and SIP, K_2 , and between SIP and CIP, K_3 [14].

The most important advantage of DRS in ion association studies is that it allows us to identify the ion-pair species relevant for the studied electrolyte system, detects possible dipolar triple ions such as $[\text{Mg}_2\text{SO}_4]^{2+}$ [41], and directly yields the corresponding species concentrations (Fig. 8b). From these concentrations, stepwise equilibrium constants, such as

$$K_1 = c_{2\text{SIP}}/c_+c_-; \quad K_2 = c_{\text{SIP}}/c_{2\text{SIP}}; \quad \text{and} \quad K_3 = c_{\text{CIP}}/c_{\text{SIP}} \quad (8)$$

for $\text{CuSO}_4(\text{aq})$ [34] or $\text{Al}_2(\text{SO}_4)_3(\text{aq})$ (Fig. 10) [14], can be immediately calculated. Such information is usually not accessible, certainly not over a wider concentration range. The few ultrasonic relaxation data for the stepwise stability constants at infinite dilution are generally in good agreement with the values for $\lim_{c \rightarrow 0} K_i$ from DRS [19,33,34,41].

CLOSING REMARKS

Although already applied in the early 1950s, DRS has long been neglected in solution chemistry. This was mainly due to the inherent experimental difficulties, restricting the technique to a few specialist groups. But also the often problematic interpretations put forward in too many previous DRS studies, neglecting common knowledge in solution chemistry, shed an unfavorable light on this technique and shadowed existing serious investigations [16]. Hopefully, the present overview will help to overcome this situation and convince the audience that DRS is indeed a useful method in solution studies.

In many aspects, such as the decomposition of the spectra or the interpretation and quantitative analysis of spectral contributions, the technique resembles more conventional spectroscopies. Differences lie in the selectivity—DRS detects the collective fluctuations of species having a permanent dipole moment and a sufficient life time. This is an advantage as DRS and, for example, infrared spectroscopy will provide complementary information, although the sensitivity toward collective modes may complicate the interpretation of dielectric spectra.

With its ability to detect 2SIP, SIP, and CIP, DRS provides direct evidence for the Eigen mechanism and closes the gap between the inference from thermodynamics (including transport studies) and molecular-level spectroscopies, such as infrared and NMR. DRS also provides information on the relative strength of ion–ion, ion–solvent, and solvent–solvent interactions in terms of the effective solvation number Z_{ib} (and eventually Z_{slow}). These data complement scattering studies and computer simulations on ion solvation.

Clearly, the strategy for the future will be to use more systematic approaches combining the various techniques, including DRS, to obtain a coherent view of increasingly complex electrolyte systems.

ACKNOWLEDGMENTS

It is a pleasure to acknowledge the collaboration and/or discussions of/with a number of colleagues on various aspects of this work: Josef Barthel, University of Regensburg, Germany; Heiner-Jakob Gores, University of Regensburg, Germany; Glenn Hefter, Murdoch University, Australia; Hartmut Krienke, University of Regensburg, Germany; Takaaki Sato, Waseda University, Japan; and of the many Ph.D. students involved in Regensburg and Murdoch over the last 15 years, especially Simon Schrödle and Wolfgang Wachter.

REFERENCES

1. J. O'M. Bockris, A. K. N. Reddy. *Modern Electrochemistry*, Vol. 1, 2nd ed., Plenum, New York (1998).
2. J. Barthel, H. Krienke, W. Kunz. *Physical Chemistry of Electrolyte Solutions*, Springer, New York (1998).
3. B. M. Rode, C. F. Schwenk, B. R. Randolf. "Classical versus quantum mechanical simulations: The accuracy of computer experiments in solution chemistry", in *Novel Approaches to the Structure and Dynamics of Liquids: Experiments, Theories and Simulations*, J. Samios, V. A. Durov, (Eds.), pp. 41–52, NATO Science Ser. II: Mathematics, Physics and Chemistry, Vol. 133, Kluwer, Dordrecht (2004).
4. H. Ohtaki, T. Radnai. *Chem. Rev.* **93**, 1157 (1993).
5. A. A. Zavitsas. *J. Phys. Chem. B* **105**, 7805 (2001).
6. J.-J. Max, C. Chapados. *J. Phys. Chem.* **115**, 2664 (2001).
7. J.-J. Max, V. Gessinger, C. van Driessche, P. Larouche, C. Chapados. *J. Chem. Phys.* **126**, 184507 (2007).
8. K. D. Collins. *Biophys. Chem.* **119**, 271 (2006).
9. F. Malatesta, R. Zamboni. *J. Solution Chem.* **26**, 791 (1997).

10. G. Hefter. *Pure Appl. Chem.* **98**, 1571 (2006).
11. Y. Marcus, G. Hefter. *Chem. Rev.* **106**, 4585 (2006).
12. F. Kremer, A. Schönhalz (Eds.). *Broadband Dielectric Spectroscopy*, Springer, Berlin (2003).
13. R. Buchner. "Dielectric spectroscopy of solutions", in *Novel Approaches to the Structure and Dynamics of Liquids: Experiments, Theories and Simulations*, J. Samios, V. A. Durov (Eds.), pp. 265–288, NATO Science Ser. II: Mathematics, Physics and Chemistry, Vol. 133, Kluwer, Dordrecht (2004).
14. S. Schrödle, W. W. Rudolph, G. Hefter, R. Buchner. *Geochim. Cosmochim. Acta* **71**, 5287 (2007).
15. R. Buchner, J. Barthel, J. B. Gill. *Phys. Chem. Chem. Phys.* **1**, 105 (1999).
16. R. Buchner, J. Barthel. *Annu. Rep. Prog. Chem.* **97**, 349 (2001).
17. M. R. Moldover, K. N. Marsh, J. Barthel, R. Buchner. "Relative permittivity and refractive index", in *Experimental Thermodynamics, Vol. VI: Measurement of the Thermodynamic Properties of Single Phases*, A. R. H. Goodwin, K. N. Marsh, W. A. Wakeham (Eds.), pp. 433–473, Elsevier, Amsterdam (2003).
18. U. Kaatze, Y. Feldman. *Meas. Sci. Technol.* **17**, R17 (2006).
19. R. Buchner, T. Chen, G. Hefter. *J. Phys. Chem. B* **108**, 2365 (2004).
20. J. Barthel, H. Hetzenauer, R. Buchner. *Ber. Bunsen-Ges. Phys. Chem.* **96**, 1424 (1992).
21. R. Buchner, C. Hölzl, J. Stauber, J. Barthel. *Phys. Chem. Chem. Phys.* **4**, 2169 (2002).
22. B. Wurm, M. Münsterer, J. Richardi, R. Buchner, J. Barthel. *J. Mol. Liq.* **119**, 97 (2005).
23. B. Wurm, C. Baar, R. Buchner, J. Barthel. *J. Mol. Liq.* **127**, 14 (2006).
24. A. Tromans, P. M. May, G. Hefter, T. Sato, R. Buchner. *J. Phys. Chem. B* **108**, 13789 (2004).
25. W. Wachter, R. Buchner, G. Hefter. *J. Phys. Chem. B* **110**, 5147 (2006).
26. U. Kaatze, R. Behrends, R. Pottel. *J. Non-Cryst. Solids* **305**, 19 (2002).
27. E. Hanke, K. von Roden, U. Kaatze. *J. Chem. Phys.* **125**, 084507 (2006).
28. T. Sato, R. Buchner. *J. Mol. Liq.* **117**, 23 (2005).
29. W. Wachter, W. Kunz, R. Buchner, G. Hefter. *J. Phys. Chem. A* **109**, 8675 (2005).
30. R. Buchner, G. Hefter. *J. Solution Chem.* **31**, 521 (2002).
31. W. Wachter, Š. Fernandez, R. Buchner, G. Hefter. *J. Phys. Chem. B* **111**, 9010 (2007).
32. T. Chen, G. Hefter, R. Buchner. *J. Phys. Chem. A* **107**, 4025 (2003).
33. T. Chen, G. Hefter, R. Buchner. *J. Solution Chem.* **34**, 1045 (2005).
34. C. Akilan, G. Hefter, N. Rohman, R. Buchner. *J. Phys. Chem. B* **110**, 14961 (2006).
35. R. Buchner, F. Samani, P. M. May, P. Sturm, G. Hefter. *ChemPhysChem* **4**, 373 (2003).
36. P. Eberspächer, E. Wismeth, R. Buchner, J. Barthel. *J. Mol. Liq.* **129**, 3 (2006).
37. A. Tromans, G. Hefter, P. M. May. *Aust. J. Chem.* **58**, 213 (2005).
38. P. Sipos, M. Schibeci, G. Peintler, P. M. May, G. Hefter. *J. Chem. Soc., Dalton Trans.* 1858 (2006).
39. (a) M. Eigen, K. Tamm. *Z. Elektrochem.* **66**, 93 (1962); (b) M. Eigen, K. Tamm. *Z. Elektrochem.* **66**, 107 (1962).
40. T. Fukasawa, T. Sato, J. Watanabe, Y. Hama, W. Kunz, R. Buchner. *Phys. Rev. Lett.* **95**, 197802 (2005).
41. C. Akilan, N. Rohman, G. Hefter, R. Buchner. *ChemPhysChem* **7**, 2319 (2006).
42. W. W. Rudolph, G. Irmer, G. Hefter. *Phys. Chem. Chem. Phys.* **5**, 5253 (2003).
43. R. A. Robinson, R. H. Stokes. *Electrolyte Solutions*, 2nd ed., Butterworth, London (1970).
44. M. Bešter-Rogač, V. Babič, T. M. Perger, R. Neueder, J. Barthel. *J. Mol. Liq.* **118**, 111 (2005).
45. K. J. Powell, P. L. Brown, R. H. Byrne, T. Gajda, G. T. Hefter, S. Sjöberg, H. Wanner. *Pure Appl. Chem.* **79**, 895 (2007).